

## Atomic structure and electronic properties of Ni<sub>3</sub>Al(111) and (011) surfaces

L. Jurczyszyn,<sup>1</sup> A. Krupski,<sup>1,2,\*</sup> S. Degen,<sup>2</sup> B. Pieczyrak,<sup>1</sup> M. Kralj,<sup>2,†</sup> C. Becker,<sup>2</sup> and K. Wandelt<sup>2</sup>

<sup>1</sup>*Institute of Experimental Physics, University of Wrocław, plac Maksa Borna 9, 50-204 Wrocław, Poland*

<sup>2</sup>*Institute of Physical and Theoretical Chemistry, University of Bonn, Wegelestrasse 12, D-53115 Bonn, Germany*

(Received 16 November 2006; published 3 July 2007)

We present results of theoretical studies of the structural and electronic properties of (111) and (011) surfaces of paramagnetic Ni<sub>3</sub>Al alloy. Atomic and electronic structures of these surfaces have been obtained from the density-functional calculations performed with the use of plane wave basis set. Our *ab initio* calculations show that for all considered surfaces, the topmost Al atoms are located above Ni atoms, and the structural parameters of relaxed surface systems well correspond to experimental data provided by earlier low-energy electron-diffraction measurements. The details of the calculated electronic structure of Ni<sub>3</sub>Al(111) in the vicinity of the Fermi level were compared with the results of scanning tunneling spectroscopy (STS) measurements which we have performed for this system, and a good agreement has been found between the calculated local-density-of-states distributions and the shape of obtained STS spectra.

DOI: 10.1103/PhysRevB.76.045101

PACS number(s): 73.20.At

### I. INTRODUCTION

The NiAl surfaces<sup>1</sup> are interesting because they are more and more often used as a substrate in experimental studies of a variety of different surface phenomena such as adsorption,<sup>2</sup> oxidation,<sup>3-6</sup> and formation of more complex systems, e.g., Cu-phthalocyanine/Al<sub>2</sub>O<sub>3</sub>/NiAl(001),<sup>7</sup> Pd/Al<sub>2</sub>O<sub>3</sub>/Ni<sub>3</sub>Al(111),<sup>8</sup> or Fe/Al<sub>2</sub>O<sub>3</sub>/Ni<sub>3</sub>Al(111).<sup>9</sup> It is therefore important to investigate atomic and electronic properties of NiAl surfaces to make a correct interpretation of the obtained experimental data and to explain the mechanism of atomic and electronic processes that take place under distinct conditions. However, until now, the number of experimental and theoretical studies related to Ni<sub>3</sub>Al surfaces is rather small. The low-energy electron-diffraction (LEED)-intensity analysis of clean (111), (001), and (011) surfaces of this alloy, performed 20 years ago by Sondericker *et al.*,<sup>10-12</sup> provided experimental data about their atomic structures. LEED measurements have shown that the surface Al atoms are in all cases located above the Ni atoms. This observation has been confirmed by structural calculations performed at the same time by Chen *et al.*<sup>13</sup> Geometrical properties of clean Ni<sub>3</sub>Al(111) have also been studied using surface x-ray diffraction;<sup>14</sup> however, these measurements were performed in the context of disorder and segregation of the considered surface system, and thus, their results cannot be compared directly with earlier LEED data.<sup>12</sup> In addition, diffusive and structural properties of Ni<sub>3</sub>Al(111) and Ni<sub>3</sub>Al(011) in the presence of adatoms and vacancies have been studied theoretically within the molecular dynamics technique.<sup>15,16</sup>

In this paper, we present a theoretical study of the structural and electronic properties of (111) and (011) surfaces of the ordered paramagnetic Ni<sub>3</sub>Al alloy. Geometries of these surfaces and their electronic structures have been obtained from first-principles pseudopotential calculations based on the density-functional theory (DFT) and the use of plane wave basis set. The experimental part of our study is connected with the Ni<sub>3</sub>Al(111) system and is based on the combination of scanning tunneling microscopy (STM)/scanning tunneling spectroscopy (STS) measurements performed for a

clean Ni<sub>3</sub>Al(111) surface, as well as for this surface covered by an Al<sub>2</sub>O<sub>3</sub> film. The obtained experimental data have been analyzed in detail with respect to the theoretical results of our *ab initio* calculations. All the obtained results have been thoroughly discussed in the context of previous experimental and theoretical studies.

Our theoretical investigations are based on the assumption that the stoichiometric composition in surface region is exactly the same as in the bulk of the alloy, which is supported by earlier theoretical and experimental studies.<sup>10,12,17</sup> Theoretical investigation of the connection between bulk stoichiometric of Ni<sub>3</sub>Al and the surface energy of its (111) surface clearly indicates that for the ideal bulk stoichiometric (i.e., 0.25 Al and 0.75 Ni), the surface composition of (111) surface is pinned to this stoichiometric value.<sup>17</sup> A low-energy-diffraction intensity analysis of a clean Ni<sub>3</sub>Al(111) surface<sup>12</sup> reveals a structure that is essentially bulklike with one Al atom and three Ni atoms per unit mesh. It follows from this consideration that such bulklike equilibrium composition is stable between room temperature and 750 °C. The same type of LEED measurements performed for (011) surface<sup>11</sup> also shows that in this case, the stoichiometric composition of the surface layer reproduces composition of the bulk (mixed-layer composition: 0.5 Al and 0.5 Ni). On the other hand, recently published results of x-ray diffraction<sup>14</sup> indicate the unexpected disorder in the surface region of clean Ni<sub>3</sub>Al(111). This disorder was discussed in Ref. 14 as a possible consequence of segregation or a small off stoichiometry at the bulk. However, the structural properties of Ni<sub>3</sub>Al(111) surface considered in Ref. 14 are significantly different than it takes place in Ref. 12 and also in our present experimental study reported in this paper where segregation effects are not observed. Therefore, we think that the use of the ideal stoichiometric model in our *ab initio* calculations is well justified and properly reflects structural properties of Ni<sub>3</sub>Al(111) which was used in our experiment.

### II. METHOD OF CALCULATION

Description of Ni<sub>3</sub>Al surfaces was done using a slab approach. Results presented in this paper were obtained for

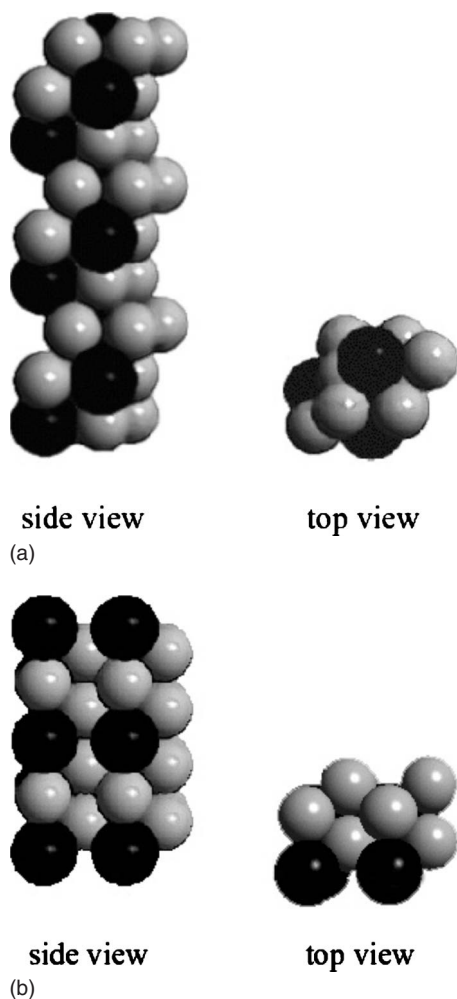


FIG. 1. (a) Schematic plot (side and top views) of the supercell used in calculations for the  $\text{Ni}_3\text{Al}(111)$  system (the slab with nine atomic layers is presented). (b) The same as in (a) but for the  $\text{Ni}_3\text{Al}(011)$  system.

repeated slab built up by 9 or 11 atomic layers with four atoms in each layer. In each case, the width of the vacuum region separating the slabs was equal to the thickness of the slab.

As it was mentioned above, our *ab initio* calculations have been performed assuming that the stoichiometry of considered surfaces of  $\text{Ni}_3\text{Al}$  alloy is the same as in its bulk, which is in agreement with previous experimental and theoretical findings.<sup>10,11,17</sup> Structure of the supercells for the (111) and (011) surfaces is schematically shown in Fig. 1. In the case of the (111) system, all the atomic planes parallel to the surface are exactly the same, with the stoichiometric composition of three Ni atoms and one Al atom [see Fig. 1(a)]. On the other hand, for the supercell corresponding to the (011) system, we deal with two types of atomic planes with 50%Ni–50%Al composition and 100%Ni composition, respectively. These two kinds of atomic planes appear in an alternating fashion along the (011) direction, as shown in Fig. 1(b). Consequently, in the case of the (011) orientation, the surface layer may contain an equal number of Ni and Al atoms (mixed-layer termination) or it may be formed by just

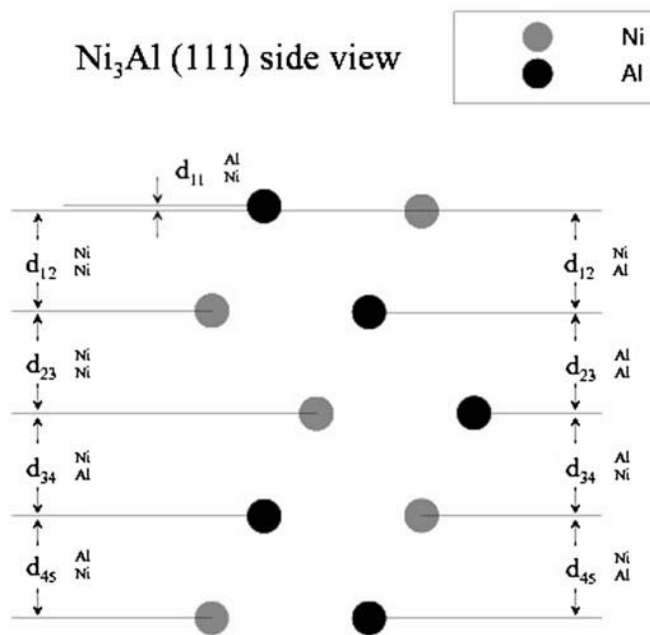


FIG. 2. Schematic side view of the relaxed  $\text{Ni}_3\text{Al}(111)$  structure. Values of the denoted characteristic interplane distances are given in Table I.

Ni atoms (Ni-layer termination). However, the LEED analysis indicates that only the mixed-layer termination occurs in reality,<sup>10,11</sup> and therefore, only this termination was considered in our paper. It means that the respective (011)-oriented slab (built up by nine atomic planes) was terminated with a mixed layer at both sides. Nevertheless, for checking purposes, we additionally tested the effect of a Ni-terminated surface at one side of the slab on the relaxation of a mixed-layer surface at the opposite slab side. In the case of the (011) surface, the results presented in this paper were obtained for a  $(2 \times 2)$  unit cell [as in Fig. 1(b)]; however, checking calculations have also been performed for a  $(1 \times 2)$  unit cell. As it was mentioned above, our *ab initio* calculations have been performed assuming that the stoichiometry of considered surfaces of  $\text{Ni}_3\text{Al}$  alloy is the same as in its bulk, which is in agreement with previous experimental and theoretical findings.<sup>10,11,17</sup>

Geometry of the ground state of the considered systems was found from the minimalization of its total energy. Simulations of the relaxation were performed in the framework of *ab initio* DFT calculations using the plane wave basis set, as implemented in the VASP package.<sup>18–20</sup> The electron-ion interactions were described by the projector-augmented wave method,<sup>21</sup> while the exchange-correlation effects were evaluated within the local-density approximation.

In the case of the (011) system, the surface Brillouin zone was sampled by a Monkhorst and Pack mesh of  $(11 \times 11 \times 1)$ , which leads to 36 irreducible  $k$  points. For the (111) surface, we have applied gamma-centered grids  $(11 \times 11 \times 1)$ , again resulting in 36 irreducible  $k$  points. However, to obtain high-quality density-of-states (DOS) distributions, a very fine  $k$  mesh has to be applied. Therefore, all DOS distributions presented in this paper have been obtained for the mesh not smaller than  $(19 \times 19 \times 1)$ .

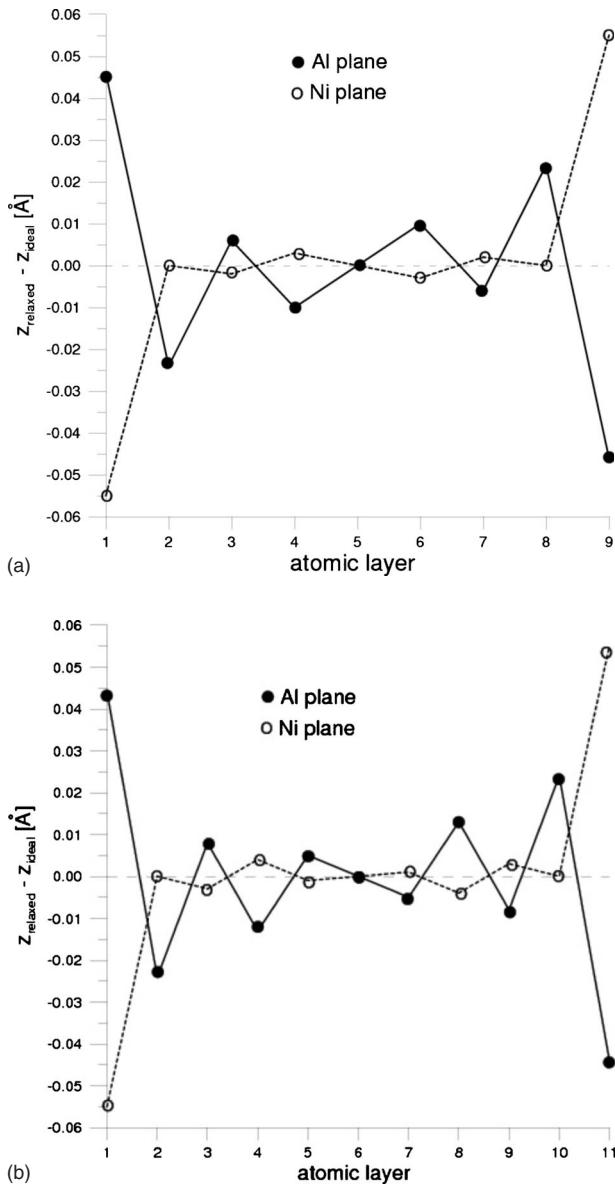


FIG. 3. Changes of the positions of atomic planes in the  $\text{Ni}_3\text{Al}(111)$  slab caused by relaxation, with respect to an ideal (unrelaxed) geometry for the slab with 9 (a) and 11 (b) layers.

In the course of computations, the energy of the electronic state was optimized using Davison-block algorithm, while conjugate-gradient algorithm was applied to relax the atomic positions. All the results presented in this paper were obtained assuming that positions of all atoms forming the slab were allowed to relax.

The lattice parameter following from the energy minimization of the  $\text{Ni}_3\text{Al}$  bulk unit cell equals to 2.463  $\text{\AA}$ . This value was next used for relaxation of the (111) and (011) slab systems.

### III. EXPERIMENTAL DETAILS

The STM/STS measurements for the  $\text{Ni}_3\text{Al}(111)$  were performed in an ultrahigh vacuum chamber with a base pressure lower than  $2 \times 10^{-8}$  Pa. The measurements were done

with a homebuilt setup utilizing a beetle-type liquid helium cooled STM. All STM measurements reported here were performed at 23 K. The bias voltage was applied to the sample. STS measurements were done using a lock-in amplifier to detect the differential conductance. Modulation frequencies in the range of 5–10 kHz and amplitudes between 10 and 60 mV were used. The  $\text{Ni}_3\text{Al}(111)$  single crystal was obtained from MaTeck. Cleaning of the  $\text{Ni}_3\text{Al}(111)$  surface was done by repeated cycles of Ar-ion sputtering at a sample temperature of 600 K (15 min, 2.5 keV,  $9.5 \mu\text{A}/\text{cm}^2$ ) with subsequent annealing at 1150 K (7 min) and 1000 K (7 min). The alumina films were grown by oxidation of the clean surface at 1000 K at an oxygen partial pressure of  $3 \times 10^{-6}$  Pa. After an  $\text{O}_2$  exposure of 40 L, dosing was stopped, and the sample was annealed at 1050 K for 5 min. This oxidation process was performed two times to obtain closed and long-range-ordered alumina films. Some of the presented experimental STM images were slightly filtered using a Fourier filter. The STM data were processed using a freeware image-processing software.<sup>22</sup>

## IV. RESULTS AND DISCUSSION

### A. $\text{Ni}_3\text{Al}(111)$

Within the theoretical part of our work related to the clean  $\text{Ni}_3\text{Al}(111)$ , we have calculated multilayer relaxations of the slab with 9 and 11 atomic layers. Our structural *ab initio* calculations indicate that relaxation process causes remarkable changes of vertical positions of both Al and Ni atoms within atomic planes located close to the  $\text{Ni}_3\text{Al}(111)$  surface. A sketch of the relaxed  $\text{Ni}_3\text{Al}(111)$  structure is shown in Fig. 2, while the corresponding interatomic distances characterizing the relaxed structure and their relative changes with respect to an ideal unrelaxed structure are gathered in Table I. This table also compares our present theoretical results with LEED data<sup>10,12</sup> and the results of previous theoretical study.<sup>13</sup> Modifications of the atomic coordinates along directions parallel to the surface plane are found to be rather small (less than 0.003  $\text{\AA}$ ) and therefore are not specified in Table I. We have found a surface rippling of 0.1  $\text{\AA}$  at the topmost atomic layer, with the surface Al atoms shifted out while the surface Ni atoms shifted in. This result is in agreement with LEED-intensity analysis of a clean (111) surface of  $\text{Ni}_3\text{Al}$  alloy<sup>10,12</sup> and with the other theoretical study.<sup>13</sup>

As concerns the deeper atomic layers, our results indicate the presence of long-range oscillatory relaxations. This effect is illustrated in Figs. 3(a) and 3(b) by showing the changes of the vertical positions of Al and Ni atoms at different atomic layers (with respect to the ideal structures) for the 9- and 11-layer slabs, respectively. Within the third and fifth layers, Al atoms are located higher (i.e., closer to the surface) than Ni atoms, as in the surface layer, while the opposite holds for the second and fourth layers. Consequently, the character of rippling of the subsequent atomic layers changes in an oscillatory manner. Similar effect has been reported by Chen *et al.*<sup>13</sup> for the case of surface relaxation of the  $\text{NiAl}(011)$  system. The amplitude of these oscillations decays into the bulk; however, this decay is nonmonotonic, as the rippling ampli-

TABLE I. Distances between atomic planes of the relaxed Ni<sub>3</sub>Al(111) system, and their relative (percentage) changes with respect to an ideal (unrelaxed) structure, calculated for the slab with 9 and 11 atomic layers. Our results are compared with the corresponding values given by LEED measurements (Ref. 12) and previous theoretical study (Ref. 13). Notation of interplane distances as in Fig. 2.

$d_{n,m}$	9 layers		11 layers		LEED (Ref. 12)		Chen <i>et al.</i> (Ref. 13)	
	(Å)	(%)	(Å)	(%)	(Å)	(%)	(Å)	(%)
Bulk value	2.011				2.055			
$d_{11}^{\text{AlNi}}$	0.100		0.098		0.06		0.07	
$d_{12}^{\text{NiNi}}$	1.956	-2.73	1.957	-2.70				
$d_{12}^{\text{AlNi}}$	2.056	2.26	2.055	2.19				
$d_{12}^{\text{AlAl}}$	2.080	3.45	2.079	3.40	2.105	2.40		3.18
$d_{12}^{\text{NiAl}}$	1.980	-1.54	1.981	-1.50	2.045	-0.48		-0.33
$d_{22}^{\text{AlNi}}$	-0.024		-0.024					
$d_{23}^{\text{NiNi}}$	2.013	0.11	2.014	0.15				
$d_{23}^{\text{AlNi}}$	1.989	-1.08	1.990	-1.05				
$d_{23}^{\text{AlAl}}$	1.981	-1.49	1.979	-1.60				
$d_{23}^{\text{NiAl}}$	2.005	-0.30	2.003	-0.39				
$d_{33}^{\text{AlNi}}$	0.008		0.011					
$d_{34}^{\text{NiNi}}$	2.006	-0.24	2.004	-0.35				
$d_{34}^{\text{AlNi}}$	2.014	0.17	2.015	0.19				
$d_{34}^{\text{AlAl}}$	2.027	0.83	2.032	1.06				
$d_{34}^{\text{NiAl}}$	2.019	0.40	2.021	0.52				
$d_{44}^{\text{AlNi}}$	-0.013		-0.017					
$d_{45}^{\text{NiNi}}$	2.014	0.15	2.017	0.28				
$d_{45}^{\text{AlNi}}$	2.001	-0.48	1.999	-0.59				
$d_{45}^{\text{AlAl}}$	2.001	-0.48	1.992	-0.93				
$d_{45}^{\text{NiAl}}$	2.001	-0.48	2.017	0.28				
$d_{55}^{\text{AlNi}}$			0.003					
$d_{56}^{\text{NiNi}}$			2.010	-0.36				
$d_{56}^{\text{AlNi}}$			2.017	0.30				
$d_{56}^{\text{AlAl}}$			2.017	0.30				
$d_{56}^{\text{NiAl}}$			2.017	0.30				

tude decays faster for layers with Al atoms located higher (cf. the first, third, and fifth layers) than it does for layers with Ni atoms located higher (cf. the second, fourth, and sixth layers).

Figure 4(a) presents a sequence of local-density-of-states (LDOS) distributions calculated at the topmost (thick solid line) and two subsequent subsurface atomic layers (thin dotted and dashed lines, respectively), as well as the corresponding distribution for the bulk layer (thin solid line). All the distributions shown in Fig. 4(a) represent a sum of LDOS contributions connected with three Ni atoms and one Al atom from the (2×2) unit cell of the corresponding layer. Figure 4(b) presents the comparison of LDOS distributions connected with three surface Ni atoms (solid line) and Al surface atom (dashed line) from the considered (2×2) surface unit cell. The LDOS components of *s-p* and *d* states of the surface Ni and Al atoms are shown in Figs. 4(c) and 4(d), respectively. These dependences indicate that for the energy range from -3 up to 0 eV, the LDOS distribution of the

Ni<sub>3</sub>Al(111) surface is dominated by the features connected with *d* states of the surface Ni atoms.

In the next step, we have compared the calculated electronic structure of Ni<sub>3</sub>Al(111) with experimental data obtained from our STM/STS measurements<sup>23</sup>. Within the experimental part of our work, we have considered a clean Ni<sub>3</sub>Al(111) surface, as well as this surface covered by Al<sub>2</sub>O<sub>3</sub> film.

It follows from our previous experimental and theoretical studies<sup>24</sup> that the topographies of Ni<sub>3</sub>Al(111) STM images are strongly influenced by intra-atomic *s-p<sub>z</sub>* interference. This kind of interference increases the efficiency of electron tunneling through *s* and *p<sub>z</sub>* orbitals of the surface Al atoms, while reducing considerably the corresponding current contributions flowing through the surface Ni atoms. Our earlier studies indicate that this factor may be responsible for the domination of surface Al atoms in STM images. In particular, we found that even for an unrelaxed surface structure, where surface Al and Ni atoms have the same vertical posi-

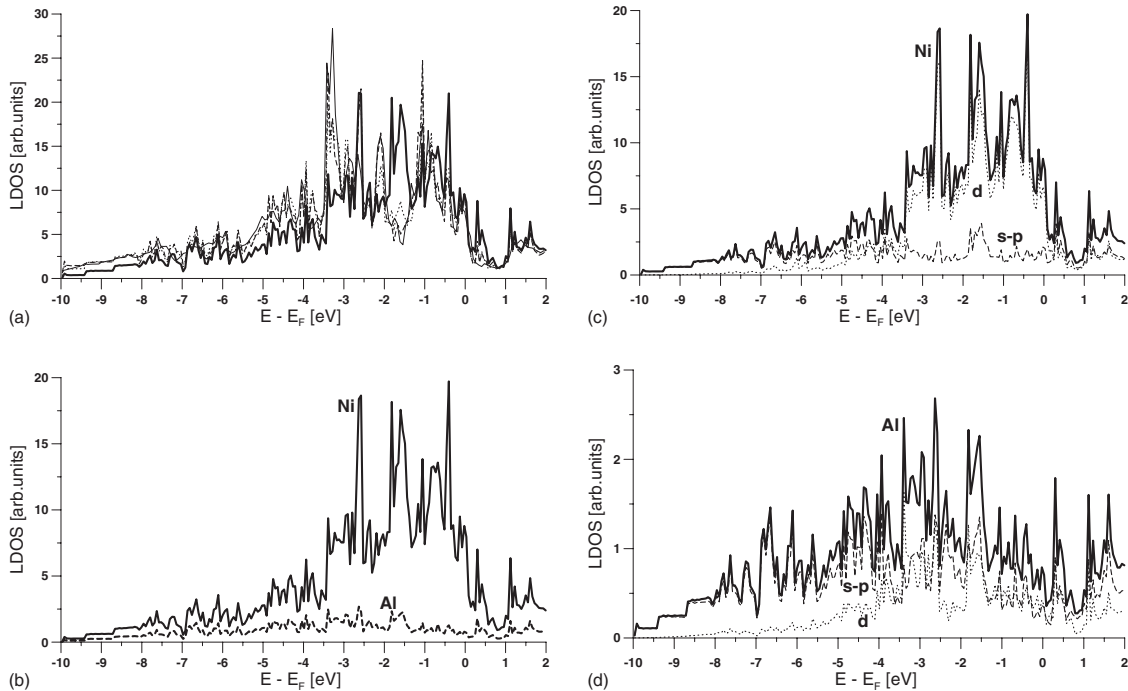


FIG. 4. (a) Total LDOS distributions at the surface layer of  $\text{Ni}_3\text{Al}(111)$  (thick solid line), and the two subsequent subsurface layers (thin dotted and dashed lines, respectively). For comparison, the corresponding distribution at the bulk layer is also shown (thin solid line). All these distributions represent the sum of LDOS contributions connected with one Al atom and three Ni atoms from the  $(2 \times 2)$  unit cell of the corresponding layer. (b) LDOS distributions connected with three Ni atoms (solid line) and one Al atom (dashed line) from the  $(2 \times 2)$  unit cell of the surface layer of  $\text{Ni}_3\text{Al}(111)$ . (c) LDOS contribution connected with Ni atoms from the  $\text{Ni}_3\text{Al}(111)$  surface layer (solid line) and its components built up by  $s$ - $p$  and  $d$  states of surface Ni atoms (dashed and dotted lines, respectively). (d) The same as in (c) but for the surface Al atom.

tions (as it takes place in the bulk), the topography of calculated STM image is dominated by Al atoms. More specifically, the surface Al atoms appear in the simulated STM images of the  $(2 \times 2)$  superstructure with the same shape and size as they appear in experimental STM data, while the surface Ni atoms are completely invisible. In the real relaxed  $\text{Ni}_3\text{Al}(111)$  surface structure, the domination of Al atoms in STM images is additionally supported by the differences in vertical positions of Al and Ni atoms.

The STM image of a clean  $\text{Ni}_3\text{Al}(111)$  surface obtained from our present measurements<sup>23</sup> is shown in Fig. 5(a). Taking into account the results of our previous study,<sup>24</sup> the topography of this image is interpreted here as a  $(2 \times 2)$  superstructure built up by surface Al atoms. Surface Ni atoms are not visible in this image; nevertheless, as it was shown in our previous study,<sup>24</sup> this fact is not in contradiction with the bulklike stoichiometric composition of the surface layer. However, instead of a long-range periodicity, the STM image shows a composition of relatively small domains with a well-visible  $(2 \times 2)$  order [see Fig. 5(a)]. The detailed study presented in Ref. 25 indicates that such a short-range order of the surface structure is an intrinsic property of the  $\text{Ni}_3\text{Al}(111)$  system. This is also well illustrated by filtered STM image shown in Fig. 5(b).

Figure 5(c) shows the STS spectra obtained for five different horizontal positions of the tip, marked by arrows in Fig. 5(a). This set of spectra indicates that, except for the maximum located at the Fermi level, the energies of the rest

of STS features dominating in the considered energy range somewhat depend on the position of the STM tip. Apart from the experimental data, Fig. 5(b) also presents the LDOS distribution at the surface layer obtained from our present *ab initio* calculations (solid line). We would like to stress out here that in the standard STS measurements, the obtained spectra mainly reflect the energy distributions of  $s$  and  $p$  states of the substrate surface, as  $d$  states are not very active during the tunneling process. Therefore, for the comparison with experimental results, the LDOS distribution plotted in Fig. 5(c) takes into account only the contributions connected with  $s$  and  $p$  states of the surface atoms. This theoretical result represents the averaged LDOS distribution over three Ni and one Al atoms from the considered  $(2 \times 2)$  surface unit cell. Below the Fermi level, theoretical distribution indicates the presence of LDOS features located 0.4 eV and 0.6 eV below  $E_F$ . The lower one (at  $-0.6$  eV) well corresponds with a distinct STS peak appearing around  $-0.6$  eV in each experimental curve. However, the higher theoretical feature (at  $-0.4$  eV) can only be linked with a relatively weak shoulder, which can be noticed in STS spectra 1, 2, and 4 around  $-0.4$  eV. Dependences presented in Fig. 5(c) also indicate that theoretical result well reproduces the measured STS features in the vicinity of the Fermi level. For unoccupied states, the calculated LDOS distribution shows a distinct feature located around 0.35 eV. Such a feature can be found in STS spectra 2 and 5, though in spectrum 2 it is somewhat shifted toward higher energies. Much weaker maxima within this energy range can also be noticed in curves 1 and 3.

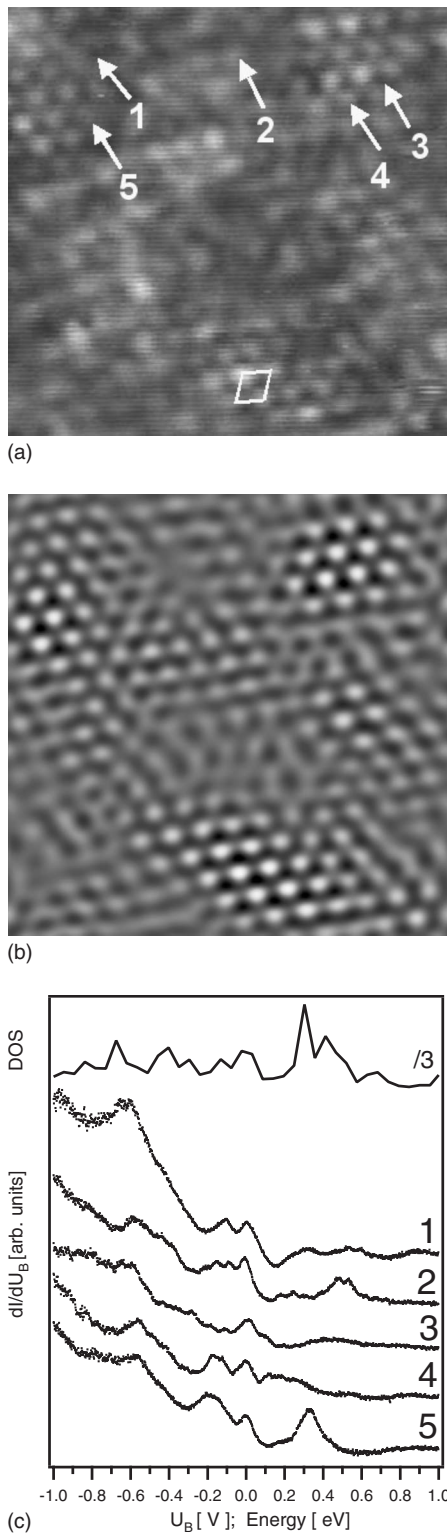


FIG. 5. (a) STM image ( $75 \times 75 \text{ \AA}^2$ ) of the clean Ni<sub>3</sub>Al(111) surface, measured at  $I_T=260 \text{ pA}$ ,  $U_{bias}=50 \text{ mV}$ , and  $T_{STM}=23 \text{ K}$ . The  $(2 \times 2)$  unit cell is indicated. (b) Filtered STM image (a) using Fourier filter. (c) Tunneling spectra measured at the points indicated on the STM image in (a). Curves 1–5 were acquired after the feedback loop was opened at 85 mV at a tunneling current of 120 pA. The corresponding modulation frequency was 5 kHz with an amplitude of 20 mV. Solid line shows the DOS calculated for the Ni<sub>3</sub>Al(111) surface.

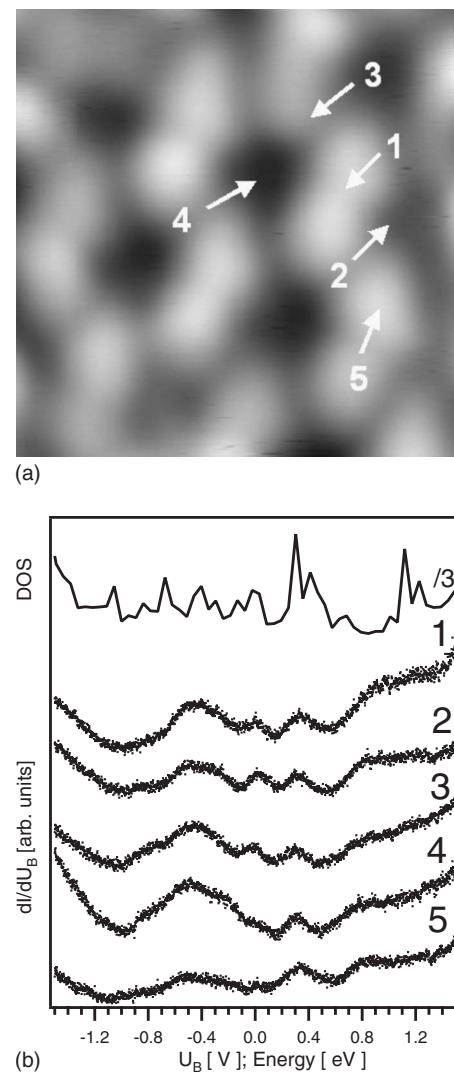


FIG. 6. (a) STM image ( $71 \times 71 \text{ \AA}^2$ ) of the Al<sub>2</sub>O<sub>3</sub>/Ni<sub>3</sub>Al(111) system, measured at  $I_T=72 \text{ pA}$ ,  $U_{bias}=3.21 \text{ V}$ , and  $T_{STM}=23 \text{ K}$ . (b) Tunneling spectra measured at the points indicated on the STM image in (a). Curves 1–5 were acquired after the feedback loop was opened at 190 mV at a tunneling current of 71 pA. The corresponding modulation frequency was 5 kHz with an amplitude of 20 mV. Solid line shows the DOS calculated for the Ni<sub>3</sub>Al(111) surface.

However, as it was mentioned, the experimental studies of Ni<sub>3</sub>Al(111) indicate the lack of the long-range order along this surface [see Figs. 5(a) and 5(b)] while the theoretical study has been performed assuming ideal translation symmetry—this fact has to be taken into account during the comparison of STS spectra and LDOS distributions presented in Fig. 5(c).

Our previous STM/STS study shows<sup>25</sup> that for the Al<sub>2</sub>O<sub>3</sub>/Ni<sub>3</sub>Al(111) system, the ordering of the substrate underneath the oxide film is much higher than for the clean Ni<sub>3</sub>Al(111) surface. The STS data indicate the presence of large oxide band gap<sup>25–28</sup> which gives an opportunity to perform the STM/STS measurements of the Ni<sub>3</sub>Al(111) substrate surface through the oxide film. In this work, we present STS spectra of Al<sub>2</sub>O<sub>3</sub>/Ni<sub>3</sub>Al(111) system obtained under such conditions. Figure 6(a) shows the STM image of

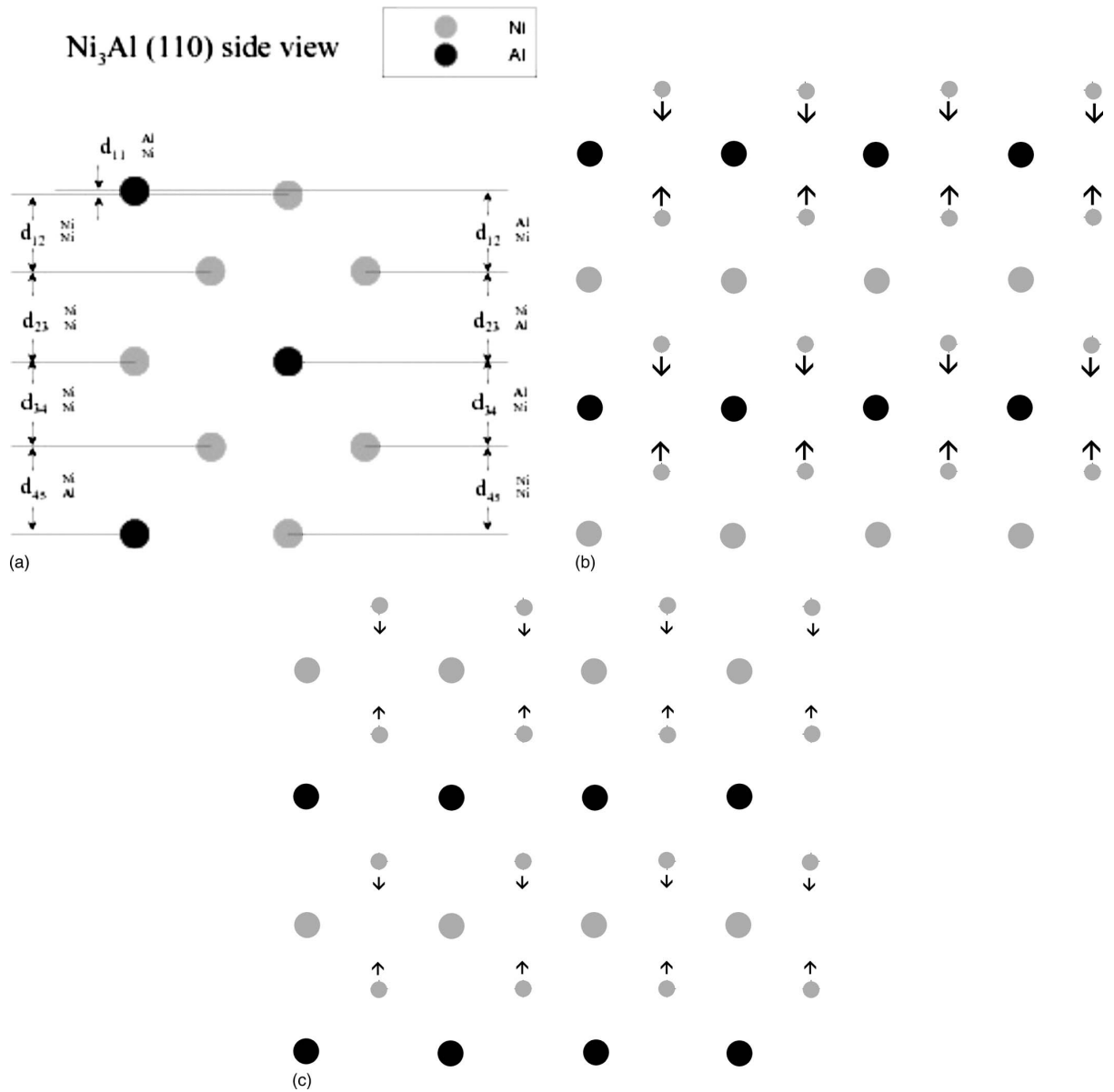


FIG. 7. (a) Schematic side view of the relaxed Ni<sub>3</sub>Al(011) structure. Values of the denoted characteristic interplane distances are given in Table II. (b) Top view of the ideal surface and the subsurface layers. Large black and gray circles denote surface Al and Ni atoms, respectively, while small gray circles represent subsurface Ni atoms. Arrows indicate the direction of the horizontal shift of subsurface Ni atoms caused by the relaxation. (c) The same as in (b) but for the third and fourth layers.

Al<sub>2</sub>O<sub>3</sub>/Ni<sub>3</sub>Al(111) received with the bias of 3.2 V, i.e., when the topography of the image is dominated by the details of the Al<sub>2</sub>O<sub>3</sub> structure. However, the set of STS spectra presented in Fig. 6(b) was obtained for the bias ranging from -1.5 up to 1.5 V, which corresponds to the energy gap of the oxide. Since for such voltages the Al<sub>2</sub>O<sub>3</sub> film seems to be invisible in STM/STS measurements,<sup>25</sup> reduction of the tip-sample separation enabled us to detect the details of the electronic structure of the Ni<sub>3</sub>Al(111) substrate. Figure 6(b) shows a set of STS spectra measured at five different horizontal positions of the STM tip, marked by arrows in Fig. 6(a). This sequence of dependences shows that, contrary to the case of a clean Ni<sub>3</sub>Al(111) [see Fig. 5(c)], the STS spectra are now almost independent of the horizontal position of

the tip. The solid line in Fig. 6(b) denotes the calculated LDOS distribution built up by *s* and *p* states of the clean Ni<sub>3</sub>Al(111) surface (only these states contribute significantly to the tunneling current). This theoretical result, obtained for a clean substrate surface, compares very well with the tunneling spectra. Indeed, the STS features appearing at -0.4, 0.0, and 0.35 eV are reproduced in the calculated LDOS distribution. Moreover, the small shoulder visible in STS data around 0.7 eV below the Fermi level (see curves 2, 3, and 4) can be connected with the LDOS maximum located also around -0.7 eV. On the other hand, the sharp LDOS peak seen at 1.1 eV in theoretical result may be linked with the broad maximum in curve 3 or the corresponding shoulders in the other STS spectra. Summarizing, we may say that for

TABLE II. Distances between atomic planes of the relaxed  $\text{Ni}_3\text{Al}(011)$  system, and their relative (percentage) changes with respect to an ideal (unrelaxed) structure. Our results are compared with the corresponding values given by LEED measurements (Ref. 12) and previous theoretical study (Ref. 13). Notation of interplane distances as in Fig. 7.

$d_{n,m}$	9 layers		11 layers		LEED (Ref. 12)		Chen <i>et al.</i> (Ref. 13)	
	(Å)	(%)	(Å)	(%)	(Å)	(%)	(Å)	(%)
Bulk value	1.232				1.259			
$d_{11}^{\text{AlNi}}$	0.055		0.037		0.015			
$d_{12}^{\text{NiNi}}$	1.081	-12.28	1.080	-12.34	1.110	-11.90		3.0
$d_{12}^{\text{AlNi}}$	1.136	-7.80	1.137	-7.70	1.125	-10.70		1.5
$d_{23}^{\text{NiNi}}$	1.280	3.90	1.279	3.83	1.300	3.20		
$d_{23}^{\text{NiAl}}$	1.285	4.34	1.287	4.47				
$d_{33}^{\text{AlNi}}$	-0.005		-0.008					
$d_{34}^{\text{NiNi}}$	1.212	-1.59	1.213	-1.52	1.260	0.08		
$d_{34}^{\text{AlNi}}$	1.207	-2.0	1.205	-2.16				
$d_{45}^{\text{NiNi}}$	1.237	0.40	1.244	0.97				
$d_{45}^{\text{NiAl}}$	1.237	0.40	1.238	4.79				
$d_{55}^{\text{AlNi}}$	-0.005		0.006					
$d_{56}^{\text{NiNi}}$	1.212	-1.59	1.225	-0.58				
$d_{56}^{\text{AlNi}}$	1.207	-2.0	1.231	-0.08				
$d_{67}^{\text{NiNi}}$	1.237	0.40	1.228	0.34				
$d_{67}^{\text{NiAl}}$	1.237	0.40	1.228	0.34				

energies within the oxide band gap, the presence of the oxide film does not modify much the surface electronic structure of the substrate, as compared to the corresponding results for a clean  $\text{Ni}_3\text{Al}(111)$  surface.

### B. $\text{Ni}_3\text{Al}(011)$

In the case of (011)-oriented slab, our theoretical study was only related to the mixed-layer termination with 50%Ni-50%Al surface atomic composition, since only this termination, as a more stable one, appears in real surface systems. Figure 7 schematically shows the relaxed  $\text{Ni}_3\text{Al}(011)$  structure. Again, the structural calculations have been performed for the slab built up by 9 or 11 atomic layers. Results obtained for both cases are very similar to each other. The calculated interatomic distances along the direction perpendicular to the surface are presented in Table II, together with their relative changes with respect to an unrelaxed structure. This table also presents the comparison of our theoretical results with experimental LEED data<sup>11</sup> and the results of previous calculations.<sup>13</sup> The ground-state geometry of the  $\text{Ni}_3\text{Al}(110)$  system provided by our present structural calculations is in good agreement with experimental LEED data.<sup>11</sup> In the case of the surface atomic layer, a relatively large contraction has been found, equal to 12.24% and 7.77% for the planes formed by surface Ni and Al atoms, respectively, which means that the surface Al atoms are located 0.055 Å above the surface Ni atoms. The same effect is indicated by LEED measurements, and the corresponding experimental values are equal to 11.9% and 10.7%. On the other hand, this result is in contradiction with earlier theoretical results ob-

tained by Chen *et al.*,<sup>13</sup> who have found 3.0% contraction for surface Ni atoms and 1.5% expansion for surface Al atoms. Our theoretical results also confirmed an increase of the separation  $d_{23}$  between the second and third layers, indicated by LEED. We have found that  $d_{23}$  increased by 3% with respect to an unrelaxed structure, while the corresponding experimental value is 3.2%. Our structural calculations indicated that Ni atoms are located slightly above Al atoms within the subsequent mixed layer (i.e., the third layer); however, the difference between their vertical positions is very small.

We have also found that the relaxation process shifts the horizontal positions of Ni atoms in the subsurface layer

TABLE III. Horizontal shifts along the  $[0\bar{1}1]$  direction of Ni atoms in different atomic layers. Latt. denotes the lattice parameter (equal to 2.463 Å).

	9 layers		11 layers	
	$\Delta Y$ (Å)	$\Delta Y/\text{latt.} \times 100\%$	$\Delta Y$ (Å)	$\Delta Y/\text{latt.} \times 100\%$
First layer				
Second layer	$\pm 0.013$	$\pm 5.42$	$\pm 0.014$	$\pm 5.68$
Third layer				
Fourth layer	$\pm 0.004$	$\pm 0.18$	$\pm 0.006$	$\pm 0.25$
Fifth layer				
Sixth layer				
Seventh layer				

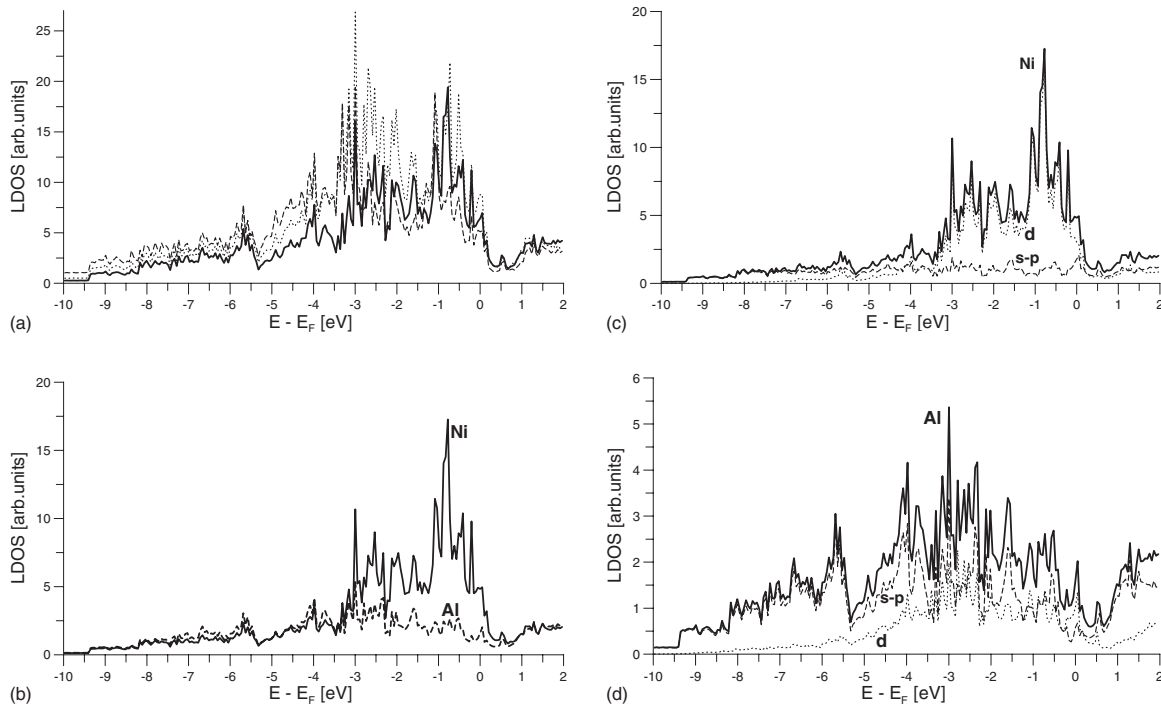


FIG. 8. (a) Total LDOS distributions at the surface layer of  $\text{Ni}_3\text{Al}(011)$  (thick solid line), and the two subsequent subsurface layers (thin dotted and dashed lines, respectively). In the case of the first and third layers (mixed layers), the corresponding dependences represent the sum of LDOS contributions connected with two Al atoms and two Ni atoms from the respective  $(2 \times 2)$  unit cell, while for the second layer, the LDOS distribution is the sum of the contributions connected with four Ni atoms. (b) LDOS distributions connected with two Ni atoms (solid line) and two Al atoms (dashed line) from the  $(2 \times 2)$  unit cell of the surface layer of  $\text{Ni}_3\text{Al}(011)$ . (c) LDOS contribution connected with Ni atoms from the  $\text{Ni}_3\text{Al}(011)$  surface layer (solid line) and its components built up by  $s$ - $p$  and  $d$  states of surface Ni atoms (dashed and dotted lines, respectively). (d) The same as in (c) but for surface Al atoms.

(100%Ni layer) along the  $[0\bar{1}1]$  direction by  $\Delta y = \pm 0.014 \text{ \AA}$ , as it is schematically shown by arrows in Fig. 7(b). This shift is correlated with the difference in vertical positions of surface Al and Ni atoms. Indeed, subsurface Ni atoms move (in the horizontal plane) toward these surface atoms which have higher vertical position, i.e., surface Al atoms [see Fig. 7(b)]. The Ni atoms from the fourth layer are shifted according to the same rule [see Fig. 7(c)] but their displacement is considerably smaller. Moreover, the Ni atoms are moved here along the  $[0\bar{1}1]$  direction toward the Ni atoms forming the upper (i.e., third) mixed layer, as shown in Fig. 7(c), since in this case, they have slightly higher vertical position than the Al atoms (see Table II). The details of the horizontal shifts of Ni atoms in different layers are gathered in Table III.

The details of the electronic structure of the  $\text{Ni}_3\text{Al}(110)$  surface are shown in Fig. 8. Figure 8(a) presents the total LDOS distributions at the surface atomic layer, which is a mixed layer (thick solid line), as well as two subsequent layers, which are 100%Ni layer (thin dotted line) and 100%Al layer (dashed line), respectively. Figure 8(b) presents the comparison between the LDOS distributions connected with two Ni surface atoms (solid line) and two Al surface atoms (dashed line) forming the  $(2 \times 2)$  unit cell, for which the calculations have been performed. The LDOS contributions connected with  $s$ - $p$  and  $d$  states of the surface Ni and Al atoms are shown in Figs. 8(c) and 8(d), respectively.

The obtained dependences show that for energies between  $-3$  and  $0$  eV, the electronic structure of the  $\text{Ni}_3\text{Al}(011)$  is dominated by  $d$  states of the surface Ni atoms. Within the rest of the considered energy range, the LDOS contributions connected with Al and Ni surface atoms are comparable.

## V. CONCLUSIONS

We have presented a theoretical study of the structural and electronic properties of (111) and (011) surfaces of paramagnetic  $\text{Ni}_3\text{Al}$  alloy assuming the bulklike stoichiometric composition in the surface region. In the case of  $\text{Ni}_3\text{Al}(111)$ , we have also performed STM/STS measurements for the clean surface, as well as for this surface covered with  $\text{Al}_2\text{O}_3$  film.

At the surface of the relaxed  $\text{Ni}_3\text{Al}(111)$  system, the plane of surface Al atoms is shifted outward, while the plane of Ni atoms is shifted inward, which leads to the difference of  $0.01 \text{ \AA}$  between vertical positions of surface Al and Ni atoms. This result is in agreement with experimental LEED data and the results of earlier structural calculations, where such a difference has also been found (equal to  $0.06$  and  $0.07 \text{ \AA}$ , respectively). Additionally, we have found that the difference in positions of Al and Ni atoms is noticeable at the deeper layers, and the rippling amplitude decays into the bulk in an oscillating manner, so that Al atoms are located above Ni atoms at the odd layers, while the opposite holds at the even layers. Our STM measurements have shown the

lack of long-range periodicity in STM images of the clean Ni<sub>3</sub>Al(111) surface, but their topographies present a composition of relatively small domains with a (2 × 2) order. The shape of STS spectra obtained from the measurements performed for the clean Ni<sub>3</sub>Al(111) somewhat depends on the horizontal position of the STM tip. Nevertheless, the calculated LDOS distribution correctly reproduces characteristic STS features in the considered energy range.

STS measurements have also been performed for the Ni<sub>3</sub>Al(111) surface covered by Al<sub>2</sub>O<sub>3</sub> film. The large oxide band gap gives an opportunity for STM/STS measurements of the Ni<sub>3</sub>Al(111) substrate surface through the oxide film. The STS spectra obtained for energies within the oxide band gap do not depend noticeably on the horizontal position of the tip and correspond very well with the LDOS distributions calculated for a clean Ni<sub>3</sub>Al(111) surface.

In the case of (011) orientation, our results of the structural calculations indicate contraction of the planes formed by surface Ni and Al atoms as large as 12.24% and 7.77%, respectively. Consequently, surface Al atoms are located

above surface Ni atoms, and the difference in their vertical positions equals to 0.055 Å. These values are in good agreement with experimental LEED data. The second interlayer spacing increased by about 4% with respect to an unrelaxed structure, which also corresponds well with LEED results. Furthermore, within the third layer, Ni atoms are located above Al atoms; however, this difference is smaller than 0.01 Å. We have also found that the relaxation process slightly modifies, along the [1 $\bar{1}$ 0] direction, the horizontal positions of Ni atoms in the subsurface layer.

#### ACKNOWLEDGMENTS

A.K. and M.K. are grateful to the Alexander von Humboldt and Hertie Foundations. A.K. was supported by the University of Wrocław under Grant No. 2016/W/IFD/2007. The financial support by the Deutsche Forschungsgemeinschaft (DFG) through SFB 624 is also gratefully acknowledged.

\*Corresponding author. FAX: +48-71-3287365  
akrupski@ifd.uni.wroc.pl

†Permanent address: Institute of Physics, P.O. Box 304, Zagreb HR-10000, Croatia.

<sup>1</sup>G. V. Nazin, X. H. Qiu, and W. Ho, *Science* **302**, 77 (2003).

<sup>2</sup>J. F. Zhu, S. F. Diaz, L. R. Heeb, and Ch. T. Cambell, *Surf. Sci.* **574**, 34 (2005).

<sup>3</sup>U. Bardi, A. Atrei, and G. Rovida, *Surf. Sci.* **239**, L511 (1990).

<sup>4</sup>U. Bardi, A. Atrei, and G. Rovida, *Surf. Sci.* **286**, 87 (1992).

<sup>5</sup>G. Kresse, M. Schmid, E. Napetschnig, M. Shishkin, L. Köhler, and P. Varga, *Science* **308**, 1440 (2005).

<sup>6</sup>S. Degen, A. Krupski, M. Kralj, A. Langner, C. Becker, M. Sokolowski, and K. Wandelt, *Surf. Sci.* **576**, L57 (2005).

<sup>7</sup>X. H. Qiu, G. V. Nazin, and W. Ho, *Phys. Rev. Lett.* **92**, 206102 (2004).

<sup>8</sup>S. Degen, C. Becker, and K. Wandelt, *Faraday Discuss.* **125**, 343 (2003).

<sup>9</sup>A. Lehnert *et al.*, *Surf. Sci.* **600**, 1804 (2006).

<sup>10</sup>D. Sondericker, F. Jona, and P. M. Marcus, *Phys. Rev. B* **33**, 900 (1986).

<sup>11</sup>D. Sondericker, F. Jona, and P. M. Marcus, *Phys. Rev. B* **34**, 6775 (1986).

<sup>12</sup>D. Sondericker, F. Jona, and P. M. Marcus, *Phys. Rev. B* **34**, 6770 (1986).

<sup>13</sup>S. P. Chen, A. F. Voter, and D. J. Srolovitz, *Phys. Rev. Lett.* **57**,

1308 (1986).

<sup>14</sup>O. Bikondoa, G. R. Castro, X. Torrelles, F. Wendler, and W. Moritz, *Phys. Rev. B* **72**, 195430 (2005).

<sup>15</sup>Ch. E. Lekka, D. G. Papageorgiou, and G. A. Evangelakis, *Surf. Sci.* **541**, 182 (2003).

<sup>16</sup>Ch. E. Lekka, D. G. Papageorgiou, and G. A. Evangelakis, *Surf. Sci.* **518**, 111 (2002).

<sup>17</sup>A. V. Ruban, *Phys. Rev. B* **65**, 174201 (2002).

<sup>18</sup>G. Kresse and J. Hafner, *Phys. Rev. B* **47**, R558 (1993).

<sup>19</sup>G. Kresse and J. Furthmüller, *Comput. Mater. Sci.* **6**, 15 (1996).

<sup>20</sup>G. Kresse and J. Furthmüller, *Phys. Rev. B* **54**, 11169 (1996).

<sup>21</sup>G. Kresse and D. Joubert, *Phys. Rev. B* **59**, 1758 (1999).

<sup>22</sup>WSXM; <http://www.nanotec.es>

<sup>23</sup>S. Degen, Ph.D. thesis, University of Bonn, 2006.

<sup>24</sup>L. Jurczyszyn, A. Rosenhahn, J. Schneider, C. Becker, and K. Wandelt, *Phys. Rev. B* **68**, 115425 (2003).

<sup>25</sup>S. Degen, A. Krupski, M. Kralj, C. Becker, and K. Wandelt (unpublished).

<sup>26</sup>S. Schintke, S. Messerli, M. Pivetta, F. Patthey, L. Libioulle, M. Stengel, A. De Vita, and W.-D. Schneider, *Phys. Rev. Lett.* **87**, 276801 (2001).

<sup>27</sup>A. Rosenhahn, J. Schneider, J. Kandler, C. Becker, and K. Wandelt, *Surf. Sci.* **433-435**, 705 (1999).

<sup>28</sup>T. Maroutian, S. Degen, C. Becker, K. Wandelt, and R. Berndt, *Phys. Rev. B* **68**, 155414 (2003).